한국해양공학회 2006년도 추계학술대회 논문집 pp. 396~402

Spline Boundary Element Modeling of Wave Scattering on a Submerged Breakwater

SUNG YOUN BOO*
* *Department of Naval Architecture, Korea Naval Academy, Chinhae, Korea*

KEY WORDS: Spline Boundary Element Method, Floating Breakwater, Submerged Horizontal Plate, Reflection Coefficient, Wave Force

ABSTRACT: *An efficient spline boundary element scheme is newly developed for water wave scattering of an incident wave train on a submerged breakwater. Validation of the present scheme is accomplished through the numerical experiments for various cases, by comparing the numerical results with theories vailable in the literature. Very accurate reflection and transmission coefficients for thin horizontal breakwater are obtained. It is observed that the reflection coefficient for the rectangular breakwater is significantly affected by the thickness. Horizontal and vertical forces on the breakwater for various thicknesses were also investigated.*

1. Introduction

This research is motivated by a desire to build a efficient breakwater to be installed in the environment where strong tidal current exists. Various types of breakwater have been constructed to protect a coastal area by reflecting back the incident waves into the sea (Cho and Kim, 1998; Kee and Kim, 1997). However, the breakwater may cause other unwanted problems if tidal current is changed by the breakwater. Among the breakwaters, floating breakwater may be very effective if its thickness is carefully chosen not to affect the tidal flow field much. Thus, horizontal breakwater with finite thickness is considered for the present work.

Two-dimensional water wave scattering of an incident wave train on the breakwater is formulated by the integral equation using the linearized boundary conditions (Boo, 2002; Chen *et. al*, 2002). A spline boundary element (SBEM) due to Boo and Lee (1996) is newly employed for the present work and the integral equation is expressed using spline elements. Here we used three different spline elements, such as, spline element with smooth surface, with discontinuity on left side, and with discontinuity on right side.

The SBEM scheme is applied to solve the flow past the circular cylinder and thin plate in the infinite fluid. It is further extended to investigate the reflection and transmission coefficients for a submerged horizontal breakwater. In addition, reflection coefficient and wave forces are examined for the various thickness of a submerged rectangular breakwater.

Corresponding author: PO Box 88-1 Jinhae, Kyungnam
055-549-1263 smartship@empal.com

2. Mathematical Formulation

We assume that wave motions are uniform in the longitudinal direction thus allowing two-dimensional analysis. Wave motions are also assumed to be small relative to the wavelength that the linear theory is applicable. We use the Cartesian coordinates (x, y) as shown in Fig. 1. The positive y-axis is in the upward vertical direction and the positive x-axis is to the right in the horizontal direction. The undisturbed free surface coincides with $y=0$. The fluid occupies the region Ω. A monochromatic incident wave train of amplitude A and angular frequency w propagate toward a submerged structure in the water of variable depth as shown Fig.1.

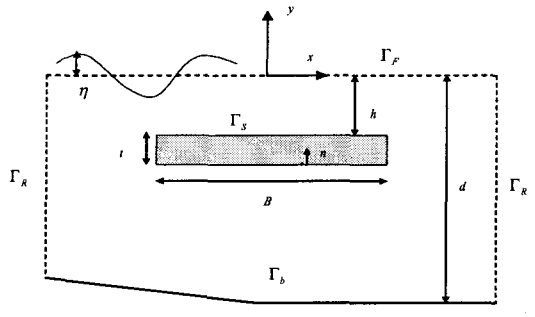

Fig. 1 Definition Sketch of wave scattering

The fluid is considered to be invicid, incompressible

and its motions are irrotational. Thus the wave field may be represented by the velocity potential $\Phi(x,y,t)$. For time harmonic motion, time term can be separated by writing the velocity potential as

$$\Phi(x,y,t) = Re\{\phi_T(x,y)e^{-i\omega t}\} \quad (1)$$

where Re is the real part, $\phi(x,y)$ is a complex spatial velocity potential, ω is the incident wave frequency, $i=\sqrt{-1}$, t denotes the time. The velocity potential $\Phi(x,y,t)$ satisfies the Laplace equation within the fluid.

$$\nabla^2\Phi(x,y,t) = 0 \quad (2)$$

The potential function $\phi(x,y)$ can be decomposed into two parts as

$$\phi(x,y) = \phi_I(x,y) + \phi_D(x,y) \quad (3)$$

where $\phi_I(x,y)$ is the known incident potential and $\phi_D(x,y)$ the diffraction potential. For the right-moving incident wave, the potential $\phi_I(x,y)$ can be represented by

$$\phi_I(x,y) = i\frac{gA}{\omega}\frac{\cosh k(y+d)}{\cosh kd}e^{ikx} \quad (4)$$

where A is the incident wave amplitude, k the wave number which satisfies the dispersion relation of

$$\omega^2 = gk\tanh(kd) \quad (5)$$

in which g is the acceleration of gravity. Also, $\phi(x,y)$ is subject to the boundary conditions of free surface Γ_F, body surface Γ_B, sea bottom Γ_b and far field boundary Γ_{R-} and Γ_{R+}.

From Eq. (1)-(3), the Laplace equation for the diffraction potentia $l\phi_D(x,y)$ is obtained as

$$\nabla^2\phi_D(x,y) = 0 \quad \text{in } \Omega \quad (9)$$

The linearized boundary conditions can be written as

$$\frac{\partial\phi_D}{\partial y} - \frac{\omega^2}{g}\phi_D = 0, \quad \text{on } \Gamma_F \quad (10)$$

$$\frac{\partial\phi_D}{\partial n} = -\frac{\partial\phi_I}{\partial n}, \quad \text{on } \Gamma_S \text{ and } \Gamma_b \quad (11)$$

$$\lim_{x\to\pm\infty}\frac{\partial\phi_D}{\partial x} \mp ik\phi_D = 0, \quad x\to\pm\infty \text{ on } \Gamma_R \quad (12)$$

In Eq. (11), n is boundary normal vector which is set to be positive pointing outside the fluid domain as shown in Fig. 1.

Once the diffraction potential $\phi_D(x,y)$ is determined, the dynamics pressure $p(x,y,t)$ can be obtained by means of the linearized Bernoulli's equation.

$$p(x,y,t) = -\rho\frac{\partial\Phi}{\partial t} = Re\{i\rho\omega\phi(x,y)e^{-i\omega t}\} \quad (13)$$

where ρ is the density of fluid. The wave forces exerting on the structure can be evaluated by integrating the fluid pressure over the wetted structure surface in the mean position.

$$f_x = i\rho\omega\iint_S(\phi_I+\phi_D)n_x ds$$

$$f_y = i\rho\omega\iint_S(\phi_I+\phi_D)n_y ds \quad (14)$$

where f_x and f_y are the force component in x and y directions, respectively. S denotes the submerged surface, and n_x and n_y the x- and y-component of the normal vector. The moment can be evaluated as

$$M_z = \iint_S p(n_y r_x - n_x r_y)ds \quad (15)$$

where $r_x = x - x_c$, $r_y = y - y_c$, and (x_c, y_c) is the moment center. When the complex potential is known, the wave profile can be determined by

$$\eta(x,y,t) = Re\left\{\frac{i\omega}{g}\phi(x,y)e^{i\omega t}\right\} \quad (16)$$

Methods to determine the reflection and transmission coefficients are reviewed in several literature. Carter (2005) derived the equations to calculate the coefficients by little modifying Chen at. al (2002) and Yueh and Kuo (1993). The resulting reflection coefficient C_R and transmission coefficient C_T due to Carter (2005) are:

$$C_R = e^{i2kx}\left[-1+\frac{k}{n_o\sinh(kd)}\int_{-d}^{0}\phi_{\Gamma_{R-}}\cosh(k(y+d))dy\right] \quad (17)$$

$$C_T = \frac{k}{n_o\sinh(kd)}\int_{-d}^{0}\phi_{\Gamma_{R-}}\cosh(k(y+d))dy \quad (18)$$

where

$$n_o = \frac{igA}{2w}\left[1+\frac{2kd}{\sinh(2kd)}\right]e^{ikx}, \quad (19)$$

$\phi_{\Gamma_{R-}}$ and $\phi_{\Gamma_{R+}}$ are the complex velocity potential $\phi(x,y)$ on Γ_{R-} and Γ_{R+}.

3. Formulation of Integral Equation

The direct boundary integral equation to solve the prescribed boundary value problems is derived by applying the Green's theorem on the boundaries. The resulting Fredholm integral equation of the second kind can be written as,

$$\tilde{C}\phi_D+\int_{\Gamma_S+\Gamma_b}\frac{\partial G}{\partial n}\phi_D d\Gamma+\int_{\Gamma_F}\left(\frac{\partial G}{\partial n}-k_0 G\right)\phi_D d\Gamma+ \quad (20)$$
$$+\int_{\Gamma_{R+}\Gamma_{R-}}\left(\frac{\partial G}{\partial n}-ikG\right)\phi_D d\Gamma=-\int_{\Gamma_S+\Gamma_b}G\frac{\partial\phi_I}{\partial n}d\Gamma$$

The solid angle $\hat{C}$ in Eq. (20) is zero when the field point is outside the boundary or 2π in the fluid domain. When the field point is located on the non-planar boundary, the solid angle is computed using a special manner. The two dimensional Green's function is:

$$G=-\frac{1}{2\pi}\ln R \quad (21)$$

where $R=\sqrt{(x-x_i)^2+(y-y_i^2)}$

4. Formulation Spline Boundary Element Method

Boundary surfaces can be modeled by distributing the elements along the surfaces. Geometries of each element can be represented by polynomial functions and thus the entire boundary surfaces can be approximated by numbers of spline elements. Within this element, physical variables are interpolated using spline polynomials. The resulting approximations on the spline element are written as:

$$x=\sum_{j=1}^{NS}N_j x_j,\quad y=\sum_{j=1}^{NS}N_j y_j \quad (22)$$

$$\phi=\sum_{j=1}^{NS}N_j\phi_j,\qquad \frac{\partial\phi}{\partial n}=\sum_{j=1}^{NS}N_j\left(\frac{\partial\phi}{\partial n}\right)_j \quad (23)$$

where (x_j,y_j),ϕ_j ,$(\partial\phi/\partial n)_j$ and N_j are the coordinates, velocity potential, normal velocity and shape function at the j-th node on each element. NS is the number of nodes on element.

The conventional higher order boundary element method (HOBEM) due to Boo (2002) has significant advantage over the constant boundary element method but the HOBEM produces inherent error in calculating the velocity or acceleration because those values are only interpolated within the element. Thus, this method may not produce continuous values of velocity or acceleration at the inter elements even on the smooth surface. This difficulty can be avoided by introducing a spline boundary element method (Boo and Lee, 2006).

Fig. 2 depicts a spline element which can be used to model a smooth surface. To drive the shape functions, we used the constraints that the derivative between elements is 0.5 and $\sum_{1}^{NS}N_j=1$. A typical shape functions for this spline element can be written as:

$$N_1(\zeta)=-\frac{1}{2}\zeta^3+\zeta^2-\frac{1}{2}\zeta$$
$$N_2(\zeta)=\frac{3}{2}\zeta^3-\frac{5}{2}\zeta^2+1 \quad (24)$$
$$N_3(\zeta)=-\frac{3}{2}\zeta^3+2\zeta^2+\frac{1}{2}\zeta$$
$$N_4(\zeta)=\frac{1}{2}\zeta^3-\frac{1}{2}\zeta^2$$

where ζ is the local coordinate defined on the element as shown in Fig. 2 and it varies from 0 to 1. This element is called as spline element type 0 (*ET 0*) for convenience.

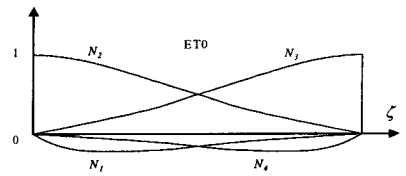

Fig. 2. Spline Element (*ET 0*)

Edges or corner can be modeled using a partially spline element. For this, we can consider two different types of element for the discontinuous boundary. Firstly, the boundary with discontinuity on the left side can be distributed by the partially spline element (*ET I*) as shown in Fig. 3. The shape function for the *ET I* can be derived below using the same constraints.

$$N_2(\zeta)=\frac{1}{2}\zeta^2-\frac{3}{2}\zeta+1$$
$$N_3(\zeta)=-\zeta^2+2\zeta \quad (25)$$
$$N_4(\zeta)=\frac{1}{2}\zeta^2-\frac{1}{2}\zeta$$

Secondly, the boundary with discontinuity on the right side can be modeled by distributing other type of partially spline element (*ET II*) as shown Fig. 4. The shape functions for this element of *ET II* can be written as:

$$N_1(\zeta) = \frac{1}{2}\zeta^2 - \frac{1}{2}\zeta$$

$$N_2(\zeta) = -\zeta^2 + 1$$

(26)

$$N_3(\zeta) = \frac{1}{2}\zeta^2 + \frac{1}{2}\zeta$$

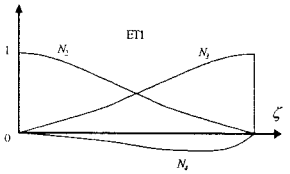

Fig. 3 Partially spline element (*ET I*)

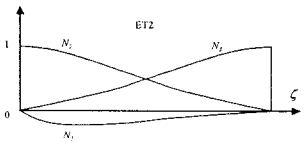

Fig. 4 Partially spline element (*ET II*)

By substituting the shape functions of Eq. (24), (25, or (26) into Eq. (20), the integral equation can be formulated for the unknown value of ϕ_D. For instance the kernels in Eq. (20) can be descretized as:

$$\int_{\Gamma_F} \Phi_D G \, d\Gamma = \sum_j^4 \int_0^1 N_j \Phi_{Dj} G \, |J| \, d\zeta$$

$$\int_{\Gamma_s} \Phi_D \frac{\partial G}{\partial n} d\Gamma = \sum_j^4 \int_0^1 N_j \Phi_{Dj} \frac{\partial G}{\partial n} |J| \, d\zeta$$

(27)

$$\int_{\Gamma_s} G \frac{\partial \Phi_I}{\partial n} d\Gamma = \sum_j^4 \int_0^1 N_j \left(\frac{\partial \Phi_I}{\partial n}\right)_j G |J| \, d\zeta$$

where

$$|J| = \sqrt{\left(\frac{dx}{d\zeta}\right)^2 + \left(\frac{dy}{d\zeta}\right)^2} \tag{28}$$

$$\frac{dx}{d\zeta} = \sum_{j=1}^{NS} \frac{\partial N_j}{\partial \zeta} x_j, \quad \frac{dy}{d\zeta} = \sum_{j=1}^{NS} \frac{\partial N_j}{\partial \zeta} y_j \tag{29}$$

5. Numerical Results and Discussions

5.1 Cylinder and Thin Plate in Infinite Fluid

Circular cylinder under the uniform flow with a velocity U in the infinite fluid is firstly considered to examine the numerical accuracy. The convergence of the velocity potential is investigated using th RMS error using

$$\text{RMS} = \sum_{i=1}^{NN} \sqrt{\frac{(\Phi_{A_i} - \Phi_{N_i})^2}{NN}} \tag{30}$$

where Φ_{A_i} and Φ_{N_i} are the analytical and numerical solution, respectively. The RMS error for the cylinder is depicted in Fig. 5. Numerical error decreases drastically as the number of elements on the surface increase. A satisfactory results may be obtained with a total element distribution of 28.

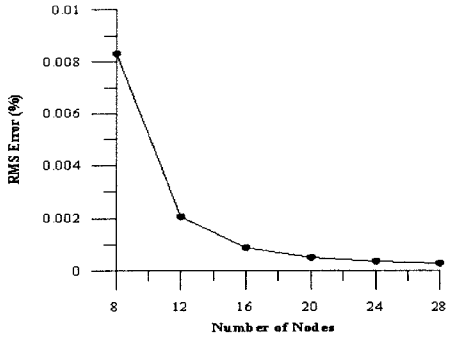

Fig. 5 RMS error of velocity potential for circular cylinder

As the 2nd example, we consider a flow past a thin flat plate with length which is perpendicular to the stream with uniform velocity U. The analytic solutions of velocity potential for zero-thickness plate can be found in several literatures. In the present modeling, a plate with thickness t is used instead of zero-thickness. The RMS error of the potential jump between weather and lee sides for the two cases of NE=10 and 20 is compared in Fig. 6. Here, NE denotes the number of elements distributed on weather or lee side of the plate. Here the total number of element used is 44 (each 20 on weather and lee sides, each 2 on the other two sides). The error is gradually reduced by decreasing the thickness of the plate. Also, the computed potential jump along the surface is compared with the analytic solution in Fig. 7. It is seen that the present SBEM solution for t/length=0.01 (NE=20) is in excellent agreement with the analytic value except the tip of the plate. This implies that zero-thickness plate may be approximated as a plate with thickness $t = 0.01 \times$ plate length and with mesh density of plate length/20 on each side. This information will be used in modeling the breakwater in the following analysis.

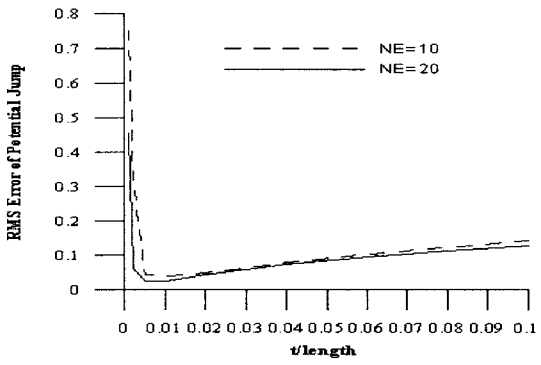

Fig. 6 RMS error of potential jump on thin plate

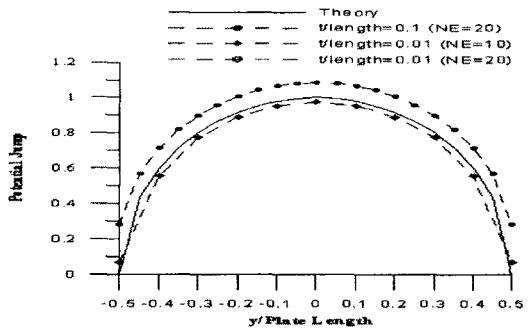

Fig. 7 Comparison of potential jump along the thin plate surface

5.2 C_R and C_T for horizontal submerged plate

A thin breakwater with length B is placed horizontally under the free surface as depicted in Fig. 1. Here, the free surface is chosen as $-5d \leq x \leq +5d$, and $B/d = 1.0$ and $h/d = 0.2$ are used. Using the previous information of thin breakwater, the number of elements used on the breakwater surface Γ_S, is 44. The fixed number of elements is also used as 100 on the bottom boundary Γ_b and 10 on each radiation boundaries Γ_{R-} and Γ_{R+}.

Convergence of the coefficients is investigated for the cases of various mesh density on the free surface. In Fig. 8, the C_R by the present method is compared with the theory of Eigen function expansion due to Cho and Kim (1998). Here the reflection coefficient C_R was calculated using Eq. (17). It can be seen that the computed C_R is in good agreement with the theory even with 8 elements/wavelength of L. However, Fig. 9 is shown the transmission coefficient C_T calculated using Eq. (18) is highly dependent on the number of element per wavelength and it converges as mesh density reaches 20 elements/L. Thus, twenty elements per wavelength are distributed on the free surface for all the following calculations.

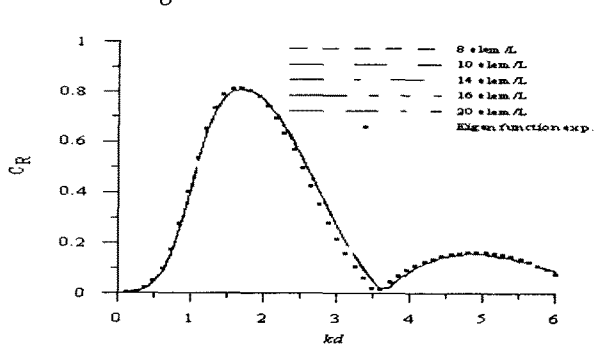

Fig. 8 Convergence of reflection coefficient

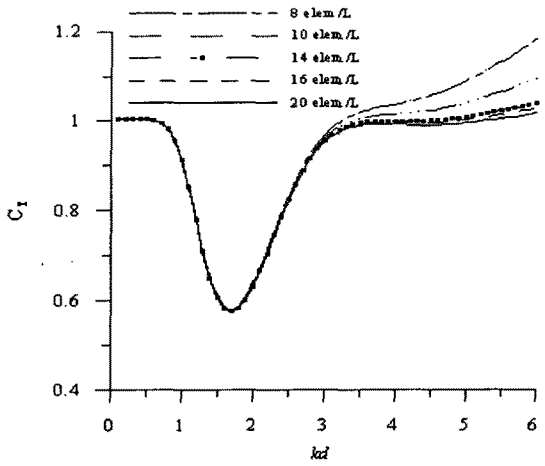

Fig. 9 Convergence of transmission coefficient

5.3 C_R and C_T for shallow water condition

Long surface waves incident on a submerged plate with zero thickness are now considered here. Under the assumption that wavelength L and breakwater length B are large compared to the water depth d, Siew and Hurley (1977) derived the equation to determined the C_R and C_T using the matched asymptotic expansions as:

$$C_R = \chi\left\{\frac{\omega B}{(gH)^{1/2}}\sin\frac{\omega B}{(gh)^{1/2}} - 2\left(\frac{h}{H}\right)^{1/2}\left(1-\cos\frac{\omega B}{(gh)^{1/2}}\right)\right\} \quad (31)$$

$$C_T = \chi\left\{2i\left[\sin\frac{\omega B}{(gh)^{1/2}} + \frac{\omega B}{b}\left(\frac{h}{g}\right)^{1/2}\right]\right\} \quad (32)$$

where,

$$\chi = 1/\left\{2\mu(1-\cos\beta) + \frac{kBH}{b}(1+\mu^2)\sin\beta + 2i\left(\sin\beta + \frac{kBH\mu}{b}\right)\cos\beta\right\} \quad (33)$$

$\beta = k_o B$, $\mu = \sqrt{h/H}$, and b is the distance under the breakwater to the sea bottom, which can be writtenas $b = d - h - t$ in the present modeling. To investigate the shallow water case, we use the parameters of $B/d = 4.0$, $h/d = 0.2$, $t = 0.001B$.

In Fig. 10, the C_R and C_T by SBEM are compared with the theories of Eq. (31) and (32). Small difference between the numerical and theoretical values is found within the shallow water range of $kd < \pi/10$, but the discrepancy becomes large as kd increases. This difference at higher kd can be expected because the theory may be valid in the range of the shallow water. However, overall trend is vary similar to each other.

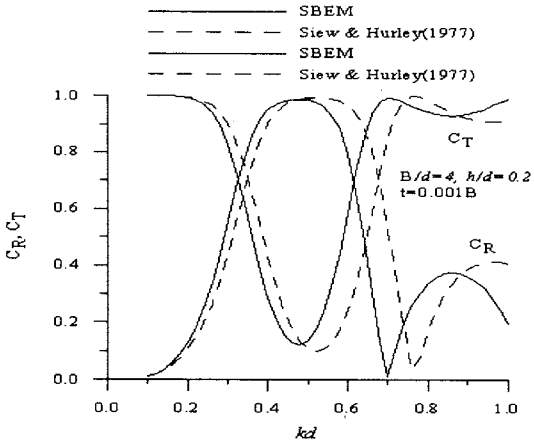

Fig. 10 Reflection and transmission coefficient for shallow water condition

5.3 Thickness Effect

Rectangular breakwaters with length B for four different thickness are considered to investigate the thickness effect on the reflection. The breakwater with length ratio of $B/d = 1.0$ is submerged at a depth of $h = 0.2d$. In Fig. 11, reflection coefficients for thickness $t = 0.001B, 0.01B, 0.1B, 0.2B$ are depicted. Difference of the coefficients for $t = 0.001B$ and $t = 0.01l$ is hardly seen, but it is observed that the coefficients decrease as the thickness increases. Therefore, the reflection coefficient depends on the thickness of the breakwater for wide range of kd and as such, the thickness of the rectangular breakwater is an important factor in modeling a breakwater. A similar result is found in Kanoria *et. al* (1999).

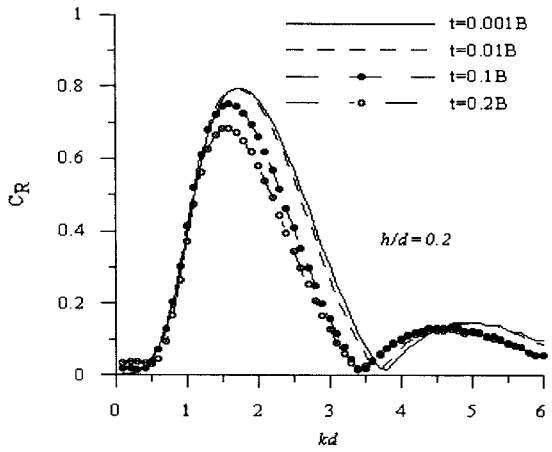

Fig. 11 Reflection coefficient for various thickness of the rectangular breakwater

5.4 Wave Forces Exerting on the Breakwater

Wave forces for the forgoing rectangular breakwater are computed. The horizontal (surge) and uplift (heave) forces normalized by ρgBA are shown in Fig. 12 and 13. As expected, surge force is much smaller than heave forces. It is seen that heave force for the smaller kd than about 2 becomes larger as the thickness increase while it becomes rather smaller when kd is greater than 2.

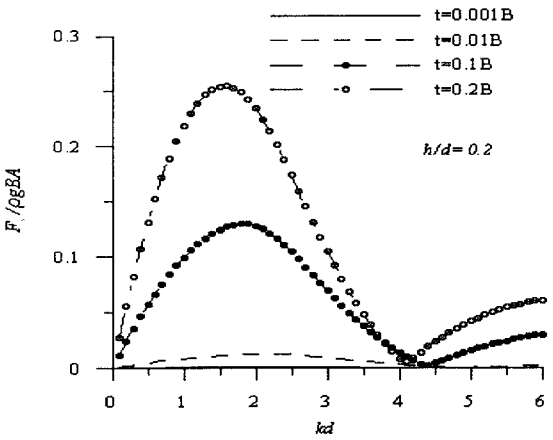

Fig. 12 Horizontal (surge) force on breakwater for various thickness

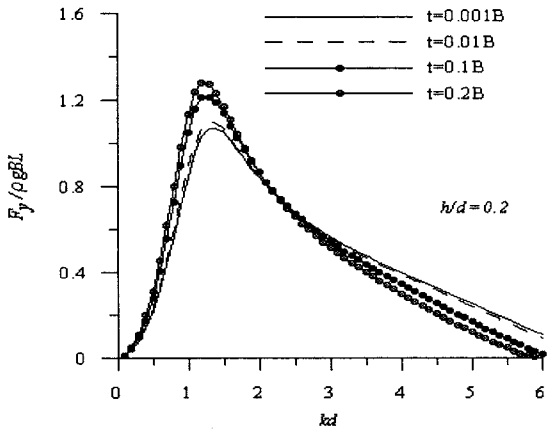

Fig. 13 Vertical (heave) force on breakwater for various thickness

6. Conclusion

An efficient spline boundary element scheme is newly developed for water wave scattering of an incident wave train on a submerged breakwater. In this scheme, three different types of spline element are employed to

model an entire boundary. Validation of the present scheme is accomplished through the numerical experiments for various cases, by comparing the numerical results with theories vailable in the literature. Very efficient and accurate reflection and transmission coefficients for thin horizontal breakwater are obtained. It is found that the reflection coefficient for the rectangular breakwater is significantly affected by the thickness and becomes smaller as the thickness increases. Horizontal and vertical forces on the breakwater for various thicknesses are also investigated.

Acknowledgement

Financial support for the Eco-Technopia 21 Project from the Korea Institute of Environmental Science and Technology (KIEST) is gratefully acknowledged.

References

Boo, S.Y. (2002). "Linear and Nonlinear Irregular Waves and Forces in a Numerical Wave Tanks", Ocean Engineering, Vo 29, pp 475-493.

Boo, S.Y. and Lee, H.M. (1996) "Application of Higher Order Spline Boundary Element Method to Two-Dimensional Lifting Problem", Proc. Annual Autumn Meeting, SNAK, Korea, pp 187-192.

Carter, R.W. (2005) "Wave Energy Converters and Submerged Horizontal Plate" M.S. Thesis, Ocean and Resources Engineering, U. of Hawaii.

Chen, K.H., Chen, J.T., Chou, C.R. and Yueh, C.Y. (2002). "Dual Boundary Element Analysis of Oblique Incident Wave Passing a Thin Submerged Breakwater", Engineering Analysis with Boundary Element, Vol 26, pp 917-928.

Cho, I.H and Kim, M.H. (1998), 'Interaction of a horizontal flexible membrane with oblique incident waves', Journal of Fluid Mechanics, Vol 367, pp 139-161

Kanoria, M., Dolar, D.P and Mandal, B.N. (1999). "Water-wave Scattering by the Thick Vertical Barriers", J. of Engineering Mathematics, Vol 35, pp 361-384.

Kee, S.T. and Kim, M.H. (1997) "Flexible Membrane Wave Barrier Part 2. Floating/Submerged buoy-membrane system", J. Waterway, Port, Coastal, and Ocean Engineering, vol 123, No 2, pp. 82-90

Seiw, P.E. and Hurley, D.G. (1977). "Long Surface Waves Incident on a Submerged Horizontal Plate", J. of Fluid Mechanics, Vol 83, pp 141-151.

Yueh, C.Y. and Kuo, Y.-Y. (1993). "The Study of Pressure and Uplift force on a Submerged Plate", Ocean Engineering, Vol 20, No 3, pp 263-280.